Dynamics of a monolayer of microspheres on an elastic substrate

S. P. Wallen,[1] A. A. Maznev,[2] and N. Boechler[1]
[1]*Department of Mechanical Engineering, University of Washington, Seattle, Washington 98195, USA*
[2]*Department of Chemistry, Massachusetts Institute of Technology, Cambridge, Massachusetts 02139, USA*
(Received 28 June 2015; published 13 November 2015)

We present a model for wave propagation in a monolayer of spheres on an elastic substrate. The model, which considers sagittally polarized waves, includes: horizontal, vertical, and rotational degrees of freedom; normal and shear coupling between the spheres and substrate, as well as between adjacent spheres; and the effects of wave propagation in the elastic substrate. For a monolayer of interacting spheres, we find three contact resonances, whose frequencies are given by simple closed-form expressions. For a monolayer of isolated spheres, only two resonances are present. The contact resonances couple to surface acoustic waves in the substrate, leading to mode hybridization and "avoided crossing" phenomena. We present dispersion curves for a monolayer of silica microspheres on a silica substrate, assuming adhesive Hertzian interactions, and compare calculations using an effective medium approximation (including elasticity of the substrate) to a discrete model of a monolayer on a rigid substrate. While the effective medium model does not describe discrete lattice effects occurring at short wavelengths, we find that it is well suited for describing the interaction between the monolayer and substrate in the long wavelength limit. We suggest that a complete picture of the dynamics of a monolayer adhered to an elastic substrate can be found by combining the dispersion curves generated with the effective medium model for the elastic substrate and the discrete model for the rigid substrate. This model is potentially scalable for use with nano- to macroscale systems, and offers the prospect of experimentally extracting contact stiffnesses from measurements of acoustic dispersion.

DOI: 10.1103/PhysRevB.92.174303 PACS number(s): 45.70.−n, 62.30.+d, 63.20.D−, 68.35.Np

I. INTRODUCTION

Granular media are simultaneously one of the most common and complex forms of matter on Earth. This complexity stems from their heterogeneous structure and highly nonlinear particulate interactions [1–3]. Over the past thirty years, mechanical wave propagation in ordered granular media has become an active field of research, as it provides an avenue to gain broader understanding of granular media dynamics [3]. Ordered granular media have also been shown to enable a wide array of novel passive wave tailoring devices that leverage the nonlinear response stemming from the Hertzian relationship between elastic particles in contact [4,5], in conjunction with the dispersion induced by periodicity [6] or local resonances [7].

The experimental configurations that are used to study mechanical wave propagation in ordered granular media typically involve spherical particles confined by elastic media. This type of arrangement is particularly common in one- and two-dimensional configurations, and includes macro- to microscale particles. For example, at the macroscale, elastic rod structures, tracks, and tubes have been used to confine the particles in one-dimensional [7–9] and quasi-one-dimensional [10] configurations, and elastic plates have been used in two dimensions [11]. More recently, the dynamics of a two-dimensional monolayer of 1 μm diameter silica particles adhered to an elastic substrate was studied using a laser ultrasonic technique [12].

Analytical models used to describe the dynamics of these systems typically only include the interaction between the particles (often just the normal Hertzian contact interaction) and disregard the effect of the substrate. In reality, even for the simple case of a particle monolayer on a substrate, more complex dynamics involving interactions between the particles and elastic waves in the substrate should be expected. Indeed, a recent experiment [12] showed that a monolayer of microspheres adhered to a substrate strongly interacts with Rayleigh surface waves in the substrate, leading to the hybridization between Rayleigh waves and a microsphere contact resonance. The results of this experiment were analyzed with a simple model involving only vertical (normal to the substrate surface) vibrations of isolated particles, following the approach adopted in earlier theoretical works on the interaction of surface oscillators with Rayleigh waves [13,14]. However, in reality, the particle motion is not confined to the vertical direction, and Rayleigh waves have a significant horizontal component. Furthermore, the interaction between neighboring particles is expected to significantly influence the dynamics.

A notable theoretical work [15] provided a model for the dynamics of crystals with adsorbed monolayers that accounted for both normal and horizontal motion and interaction between the particles, but did not take into account particle rotation. Several recent studies have demonstrated, in both theoretical [16,17] and experimental [18] contexts, that the rotational degree of freedom has a profound effect on the dynamics of ordered granular media. In particular, the study of Ref. [16] focused on the dynamics of granular monolayers (whereas Refs. [17,18] explored bulk granular structures), including cases involving interaction between the monolayer and a substrate. However, Ref. [16] only considered normal contact interactions between the particles and the substrate, and the substrate was modeled as rigid.

The aim of this work is to provide a theoretical model for the contact-based dynamics of a two-dimensional layer of spheres on a substrate, accounting for the elasticity of the substrate, translational and rotational motion of the spheres, and both normal and shear stiffnesses of sphere-to-sphere and sphere-substrate contacts. We focus on a system with

microscale particles that interact with each other and with the substrate via van der Waals adhesion forces. Rather than postulate the contact stiffness constants, we derive them from Hertzian contact models. This imposes certain constraints on the values of the constants: for example, the ratio of the normal and shear contact stiffness between the spheres is a constant only weakly dependent on the Poisson ratio. We consider contact-based modes having frequencies significantly below the intrinsic spheroidal vibrational modes of the spheres, such that they can be described as spring-mass oscillators. Furthermore, we focus on dynamics involving particle and substrate displacements in the sagittal plane, as would be detectable in a laser-based experiment [12].

We start with the case of a rigid substrate, where we find three eigenmodes involving vertical, horizontal, and rotational motion of the spheres. In the long-wavelength limit, these modes yield three contact resonances, for which simple analytical expressions are obtained. One of the resonances involves motion of the spheres normal to the substrate surface, whereas the other two involve mixed horizontal-rotational motion. We then present our effective medium model, which describes the interaction between the spheres and the substrate, and show hybridization between the contact resonances and Rayleigh surface waves. We discuss cases involving both isolated and interacting spheres, and demonstrate the important role of rotations in both cases. We also examine the validity of the effective medium approximation, by comparing calculations using discrete and effective medium models. Finally, we discuss the implications of our findings for past and future studies of granular monolayer systems.

II. MODEL

We consider a monolayer of elastic spheres on a substrate, which can be either in contact or isolated, as shown in Fig. 1(a). In either case, the spheres are assumed to form a square lattice, with the wave propagation direction aligned with the lattice vector, as shown in Fig. 1(b). We model the layer as an infinite lattice of rigid spheres with diameter $D = 2R$ and mass m, coupled to a semi-infinite, isotropic elastic substrate by normal and shear stiffnesses K_N and K_S, and to nearest-neighbor spheres by stiffnesses G_N and G_S, as schematically shown in Fig. 1(c). The subscript N corresponds to forces acting normal to the surface of the sphere, and S to forces acting transverse to the surface of the sphere. The shear springs generate an associated torque about the sphere center, while the normal springs do not. The absolute horizontal, vertical, and angular displacements of sphere j from its equilibrium state are given by Q_j, Z_j, and θ_j, respectively, and the displacements of the substrate are denoted by $u(x,z)$, corresponding to displacement in the x direction, and $w(x,z)$, corresponding to displacements in the z direction.

A. Contact stiffness

We derive the stiffnesses K_N, K_S, G_N, and G_S using Derjaguin-Muller-Toporov (DMT) [21,22] and Mindlin contact models [23]. The DMT theory is typically applicable in weakly-adhesive systems with small, stiff particles [24], and assumes that the deformation profile is Hertzian. The Mindlin

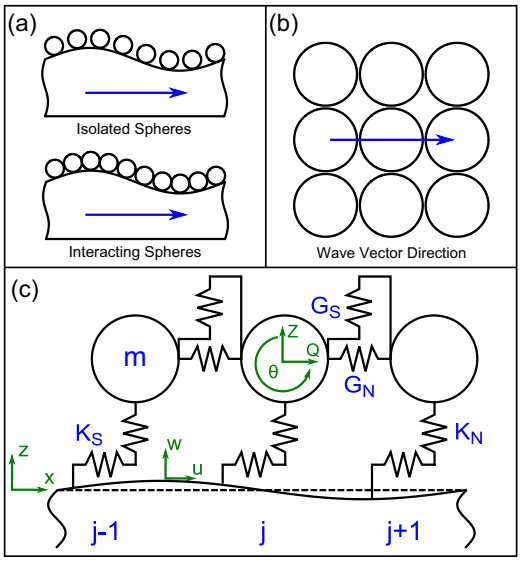

FIG. 1. (Color online) (a) Side-view schematic of an amplified wave profile for cases with isolated and interacting spheres. (b) Top-down view of the square-packed monolayer, with the arrow indicating the direction of wave propagation. (c) Schematic for the model of a monolayer of spheres coupled to an elastic half-space.

model describes the shear stiffness of particles in contact, assuming an applied normal force [23]. At the microscale, adhesive contact mechanics has been studied using atomic force microscopy and nanoindentation approaches [25].

For contact between two spheres (or a sphere and a halfspace) having elastic moduli E_1 and E_2, and Poisson ratios ν_1 and ν_2, the Hertzian restoring elastic force F_N corresponding to displacement δ_N of the particle center in the direction normal to the contact surface is given by

$$F_N = \tfrac{4}{3} E^* R_c^{1/2} \delta_N^{3/2}, \tag{1}$$

where R_c is the effective radius (equal to R for sphere-half-space contacts and $R/2$ for sphere-sphere contacts), and $E^* = [(1-\nu_1^2)/E_1 + (1-\nu_2^2)/E_2]^{-1}$ is the effective modulus. Considering the DMT adhesive force $F_{\mathrm{DMT}} = 2\pi w R_c$ acting normal to the contact surface [21,22] (where w is the work of adhesion between two surfaces), the net normal force is given by

$$F_{N,\mathrm{net}} = F_N - F_{\mathrm{DMT}}. \tag{2}$$

To describe the shear contact, we utilize the Mindlin model [23], which assumes small relative displacements and no slip at the contact surface. For two elastic bodies with shear moduli G_1 and G_2, the restoring elastic force F_S to displacement δ_S of the particle center in the direction transverse to the contact normal is given by

$$F_S = 8 G^* R_c^{1/2} \delta_S \delta_N^{1/2}, \tag{3}$$

where $G^* = [(2-\nu_1)/G_1 + (2-\nu_2)/G_2]^{-1}$ is the effective shear modulus [23]. Here, the factor of $\delta_N^{1/2}$ arises from the Hertzian relation between the contact radius and F_N given by Eq. (1).

By substituting the relative displacements $\delta_N = Z - w_0$ and $\delta_S = Q - u_0 + R\theta$ (where u_0 and w_0 are horizontal

and vertical displacements of the substrate surface at the point of contact, respectively) into Eqs. (2) and (3), and linearizing about the equilibrium configuration of $\delta_{N,0} = [3F_{\mathrm{DMT}}/(4E^* R_c^{1/2})]^{2/3}$ and $\delta_{S,0} = 0$, we derive linearized normal and shear contact stiffnesses:

$$K_N = \left(6E^{*^2} R_c F_{\mathrm{DMT}}\right)^{1/3}, \qquad K_S = 8\left(\frac{3}{4}\frac{G^{*^3}}{E^*} R_c F_{\mathrm{DMT}}\right)^{1/3}. \tag{4}$$

Stiffnesses G_N and G_S are given by equations of the same form as Eq. (4), but with E^*, G^*, R_c, and F_{DMT} adjusted for sphere-sphere contacts. In the special case where the spheres and substrate are composed of the same material, the relative magnitudes of the stiffness constants are determined exclusively by the Poisson ratio ν of the material,

$$G_N = 2^{-2/3} K_N, \quad K_S = \nu^* K_N, \quad G_S = 2^{-2/3}\nu^* K_N, \tag{5}$$

where $\nu^* = 2(1-\nu)/(2-\nu)$.

B. Equations of motion of the spheres

Assuming small displacements (i.e., Q_j, Z_j, and $R\theta_j$ are much less than D), the jth sphere obeys the equations of motion

$$\begin{aligned} m\ddot{Q}_j &= -K_S(Q_j - u_{0,j} + R\theta_j) \\ &\quad + G_N(Q_{j+1} - 2Q_j + Q_{j-1}), \\ m\ddot{Z}_j &= -K_N(Z_j - w_{0,j}) \\ &\quad + G_S[Z_{j+1} - 2Z_j + Z_{j-1} - R(\theta_{j+1} - \theta_{j-1})], \\ I\ddot{\theta}_j &= -K_S R(Q_j - u_{0,j} + R\theta_j) \\ &\quad - G_S R[R(\theta_{j+1} + 2\theta_j + \theta_{j-1}) - (Z_{j+1} - Z_{j-1})]. \end{aligned} \tag{6}$$

C. Effective medium approximation

Considering wavelengths much longer than the sphere diameter, we treat the monolayer as an effective continuous medium. By substituting the center difference formulas $[(\cdot)_{j+1} - (\cdot)_{j-1}]/(2D) \approx \partial(\cdot)/\partial x$ and $[(\cdot)_{j+1} - 2(\cdot)_j + (\cdot)_{j-1}]/(D^2) \approx \partial^2(\cdot)/\partial x^2$ into Eq. (6), we arrive at the equations of motion of the monolayer in an effective medium form:

$$\begin{aligned} m\frac{\partial^2 Q}{\partial t^2} &= -K_S(Q - u_0 + R\theta) + 4G_N R^2 \frac{\partial^2 Q}{\partial x^2}, \\ m\frac{\partial^2 Z}{\partial t^2} &= -K_N(Z - w_0) + 4G_S R^2\left(\frac{\partial^2 Z}{\partial x^2} - \frac{\partial \theta}{\partial x}\right), \\ I\frac{\partial^2 \theta}{\partial t^2} &= -K_S R(Q - u_0 + R\theta) \\ &\quad - 4G_S R^2\left(R^2\frac{\partial^2 \theta}{\partial x^2} + \theta - \frac{\partial Z}{\partial x}\right). \end{aligned} \tag{7}$$

The coupling between the monolayer and the substrate is described by the following boundary conditions at the surface $z = 0$, which describe the average force acting on the surface due to the motion of the spheres:

$$\sigma_{zx} = \frac{K_S}{A}(Q - u_0 + R\theta), \qquad \sigma_{zz} = \frac{K_N}{A}(Z - w_0), \tag{8}$$

where σ_{zx} and σ_{zz} are components of the elastic stress tensor [19] and $A = D^2$ is the area of a primitive unit cell in our square-packed monolayer. The combination of Eq. (7) and the linear elastic wave equations describing waves in the substrate [19], coupled by the boundary conditions of Eq. (8), comprises the complete effective medium model.

III. DISPERSION RELATIONS

A. Rigid substrate

1. Discrete model

We calculate the dispersion relation for a monolayer on a rigid base using Eq. (6), by assuming spatially discrete traveling wave solutions of the form $\hat{Q}e^{i(\omega t - kDj)}$ (with similar terms for the other displacements) and setting the displacements of the substrate surface $u_{0,j}$ and $w_{0,j}$ to zero. Here, $\hat{(\cdot)}$ is the amplitude of a plane wave in the displacement variable $(\cdot)$, ω is the angular frequency, and k is the wave number. After algebraic manipulation, Eq. (6) is reduced to a homogeneous system of three linear algebraic equations in terms of the amplitudes $\hat{(\cdot)}$. This system possesses nontrivial solutions only for pairs of k and ω that cause the determinant of the system to vanish. Enforcing this condition, we arrive at the following dispersion relation, where the three rows of the determinant correspond to the three equations of Eq. (6):

$$\begin{vmatrix} \frac{c_N^2}{2R^2}(1 - \cos(kD)) + \phi_S\omega_S^2 & 0 & R\omega_S^2 \\ 0 & \frac{c_S^2}{2R^2}(1 - \cos(kD)) + \phi_N\omega_N^2 & -\frac{c_S^2}{2R} i \sin(kD) \\ R\omega_S^2 & \frac{c_S^2}{2R} i \sin(kD) & \frac{I}{m}\left[\frac{c_\theta^2}{2R^2}(1 - \cos(kD)) + \phi_\theta\omega_\theta^2\right] \end{vmatrix} = 0, \tag{9}$$

where $\phi_N = 1 - \omega^2/\omega_N^2$, $\phi_S = 1 - \omega^2/\omega_S^2$, $\phi_\theta = 1 - \omega^2/\omega_\theta^2$, $c_N = \sqrt{G_N/m}(2R)$ and $c_S = \sqrt{G_S/m}(2R)$ [26], $c_\theta^2 = -mR^2c_S^2/I$, $\omega_N^2 = K_N/m$, $\omega_S^2 = K_S/m$, and $\omega_\theta^2 = (K_S + 4G_S)R^2/I$.

2. Effective medium

To obtain dispersion relations assuming an effective medium, we substitute spatially-continuous traveling wave solutions of the form $\hat{Q}e^{i(\omega t - kx)}$ (with similar terms for

the other displacements) into Q, Z, and θ in Eq. (7) with $u_0 = w_0 = 0$. Following the same procedure used to obtain Eq. (9), we obtain

$$\begin{vmatrix} c_N^2 k^2 + \phi_S \omega_S^2 & 0 & R\omega_S^2 \\ 0 & c_S^2 k^2 + \phi_N \omega_N^2 & -ikc_S^2 \\ R\omega_S^2 & ikc_S^2 & \frac{I}{m}\left(c_\theta^2 k^2 + \phi_\theta \omega_\theta^2\right) \end{vmatrix} = 0. \tag{10}$$

It is particularly instructive to examine the behavior of the effective medium model in the long wavelength limit $k \to 0$. In this limit, the displacements vary slowly in space, and the spatial derivative terms of Eq. (7) may be neglected. For the case of a rigid base, Eq. (7) reduces to the form

$$\begin{aligned} m\frac{\partial^2 Q}{\partial t^2} &= -K_S(Q + R\theta), \\ m\frac{\partial^2 Z}{\partial t^2} &= -K_N Z, \\ I\frac{\partial^2 \theta}{\partial t^2} &= -K_S R(Q + R\theta) - 4G_S R^2 \theta. \end{aligned} \tag{11}$$

The equation for Z decouples from the other two equations and yields a vertical vibrational mode. The two other equations remain coupled, yielding two modes containing both horizontal and rotational motion. Using the moment of inertia of a solid sphere $I = (2/5)mR^2$, we find three resonance frequencies

$$\begin{aligned} \omega_N &= \left(\frac{K_N}{m}\right)^{1/2}, \\ \omega_{RH} &= \left[\left(\frac{K_S}{4m}\right)(20\gamma + 7 + \sqrt{400\gamma^2 + 120\gamma + 49})\right]^{1/2}, \\ \omega_{HR} &= \left[\left(\frac{K_S}{4m}\right)(20\gamma + 7 - \sqrt{400\gamma^2 + 120\gamma + 49})\right]^{1/2}, \end{aligned} \tag{12}$$

where $\gamma = G_S/K_S$. Here, ω_N corresponds to a mode with exclusively vertical motion. The other two modes ω_{RH} and ω_{HR} exhibit both rotational and horizontal (but not vertical) motion, with relative amplitudes determined by γ. The higher of the two horizontal-rotational modes is predominantly rotational and the lower is predominantly horizontal, hence we have used the notations ω_{RH} and ω_{HR}, where the first letter in the subscript denotes the dominant motion. If the spheres and substrate are made of the same material, then, by using Eq. (5), we can relate the horizontal-rotational frequencies of Eq. (12) to the vertical resonance frequency, with the expressions $\omega_{RH} = 3.018\nu^{*1/2}\omega_N$ and $\omega_{HR} = 0.832\nu^{*1/2}\omega_N$.

In the limiting case of isolated spheres ($\gamma = 0$), ω_{RH} and ω_{HR} of Eq. (12) become $\omega_{RH,Iso} = \sqrt{7/2}\omega_S$ and $\omega_{HR,Iso} = 0$, respectively. For identical materials, $\omega_{RH,Iso} = \sqrt{7\nu^*/2}\omega_N$. The dependence of ω_{RH} and ω_{HR} on γ is shown in Fig. 2(a), where it can be seen that ω_{RH} originates at $\omega_{RH,Iso}$ for $\gamma = 0$ and grows unbounded, while ω_{HR} originates at $\omega_{HR,Iso} = 0$, and approaches ω_S asymptotically. In Fig. 2(b), we plot the horizontal and rotational displacement amplitudes as functions of γ for these two modes. Different signs of the rotational amplitude indicate that the ω_{RH} and ω_{HR} modes have different motion patterns. In the former, a positive displacement is accompanied by a counterclockwise rotation, while in the latter, it is accompanied by a clockwise rotation.

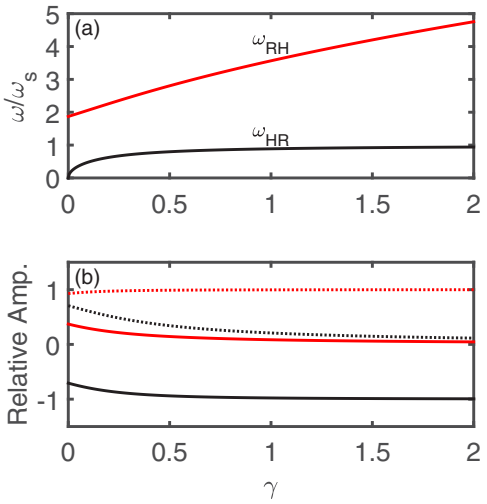

FIG. 2. (Color online) (a) Resonance frequencies ω_{RH} (red line) and ω_{HR} (black line) as functions of the stiffness ratio γ. (b) Displacement amplitudes of the resonant modes with frequencies ω_{RH} (red lines) and ω_{HR} (black lines), as functions of the stiffness ratio γ. Solid and dotted lines correspond to Q and $R\theta$, respectively. For each resonance, the amplitudes are normalized such that the sum of squares is unity. The positive sign of $R\theta$ corresponds to counterclockwise rotation.

We note that the zero-frequency mode, $\omega_{HR,Iso}$, corresponds to the rolling motion of an isolated sphere. With the inclusion of a bending rigidity, the sphere would not be allowed to freely roll, and instead would undergo rocking motion of a finite frequency. While nonzero bending rigidity exists in real systems (for instance, a microsphere adhered to a substrate does not freely roll), the frequency of resulting rocking vibrations has been shown [27,28] to be over an order of magnitude lower than the other contact resonances discussed here. Bending rigidity would thus act as a small perturbation to the predictions of our model, and we do not include it in our analysis.

To illustrate the importance of particle rotations in the model, we note that in the limiting case of $I \to \infty$, when there is no rotation, Eq. (11) yields two resonances: a vertical resonance with frequency ω_N, and a horizontal resonance having frequency ω_S. For isolated spheres, the effect of rotations can be thought of as a reduction of the "effective mass" of the sphere to $(2/7)m$, which increases the horizontal resonance frequency. On the other hand, for interacting spheres, rotations drastically change the dynamics, yielding two horizontal-rotational modes whose frequencies depend on the relative strengths of the sphere-to-sphere and sphere-substrate interactions.

B. Elastic substrate

As in the case of the effective medium approximation for a rigid substrate, we assume traveling wave solutions of the form $\hat{Q}e^{i(\omega t - kx)}$ (with similar terms for the other displacements) into Q, Z, and θ in Eq. (7). Likewise, we express the variables u_0, w_0, σ_{zx} σ_{zz} in terms of surface wave solutions

for the elastic potentials [19] $\phi(x,z,t) = \hat{\phi} e^{k\alpha z + i(\omega t - kx)}$ and $\psi(x,z,t) = \hat{\psi} e^{k\beta z + i(\omega t - kx)}$, and then substitute these expressions into Eqs. (7) and (8). Here, $\hat{(\cdot)}$ is the amplitude of a plane wave in the displacement or potential variable $(\cdot)$, $\alpha = \sqrt{1 - \omega^2/(c_L^2 k^2)}$, $\beta = \sqrt{1 - \omega^2/(c_T^2 k^2)}$, and c_L and c_T are the longitudinal and transverse sound speeds of the substrate, respectively. After algebraic manipulation, Eqs. (7) and (8) are reduced to a homogeneous system of five linear algebraic equations in the five plane wave amplitudes $\hat{(\cdot)}$, with coefficients depending on k and ω. We reach the dispersion relation by seeking nontrivial solutions of this system, which exist only for pairs of k and ω that cause the determinant of the following coefficient matrix to vanish:

$$\begin{vmatrix} ik\omega_S^2 & k\beta\omega_S^2 & c_N^2k^2 + \phi_S\omega_S^2 & 0 & R\omega_S^2 \\ -k\alpha\omega_N^2 & ik\omega_N^2 & 0 & c_S^2k^2 + \phi_N\omega_N^2 & -ikc_S^2 \\ ikR\omega_S^2 & kR\beta\omega_S^2 & R\omega_S^2 & ikc_S^2 & \frac{I}{m}\left(c_\theta^2k^2 + \phi_\theta\omega_\theta^2\right) \\ 1+\beta^2 & -2i\beta & 0 & \frac{m}{\rho A c_T^2 k^2}\left(c_S^2k^2 + \phi_N\omega_N^2 - \omega_N^2\right) & \frac{-m}{\rho A c_T^2 k^2} ikc_S^2 \\ -2i\alpha & -(1+\beta^2) & \frac{m}{\rho A c_T^2 k^2}\left(c_N^2k^2 + \phi_S\omega_S^2 - \omega_S^2\right) & 0 & 0 \end{vmatrix} = 0, \tag{13}$$

where ρ is the density of the substrate, and $A = D^2$ is the area of a primitive unit cell in our square-packed monolayer. We note that the coupling between the spheres and the substrate is represented by elements (4,4), (4,5), and (5,3) of the matrix in Eq. (13). Thus the strength of the coupling can be quantified by the ratio $m/(\rho A)$; if this term is made to vanish (e.g., by making the mass of each sphere much less than that of the portion of the substrate below it, extending to the depth of material influenced by Rayleigh waves), then the substrate and monolayer will be effectively decoupled. We note that if rotations are disregarded (e.g., by letting $I \to \infty$), Eq. (13) reduces to the same form as that of the adsorbed monolayer of Ref. [15].

It is instructive to consider the long-wave limit when the spatial derivatives in Eq. (7) can be disregarded. In this case, we find the simplified dispersion relation

$$\begin{vmatrix} ik\omega_S^2 & k\beta\omega_S^2 & \phi_S\omega_S^2 & 0 & R\omega_S^2 \\ -k\alpha\omega_N^2 & ik\omega_N^2 & 0 & \phi_N\omega_N^2 & 0 \\ ikR\omega_S^2 & kR\beta\omega_S^2 & R\omega_S^2 & 0 & \frac{I}{m}\phi_\theta\omega_\theta^2 \\ 1+\beta^2 & -2i\beta & 0 & \frac{m}{\rho A c_T^2 k^2}\left(\phi_N\omega_N^2 - \omega_N^2\right) & 0 \\ -2i\alpha & -(1+\beta^2) & \frac{m}{\rho A c_T^2 k^2}\left(\phi_S\omega_S^2 - \omega_S^2\right) & 0 & 0 \end{vmatrix} = 0. \tag{14}$$

For isolated spheres, there is no approximation in Eq. (14) with respect to Eq. (13), because, in this case, the terms generated by the spatial derivatives in Eq. (7) are identically zero. For interacting spheres, the accuracy of dispersion relations calculated with Eq. (14) will be assessed below by a comparison with results obtained with Eq. (13). We will see that Eq. (14) essentially describes the interaction of contact resonances given by Eq. (11) with Rayleigh surface waves.

IV. NUMERICAL RESULTS AND DISCUSSION

In the following calculations, we consider silica spheres of 1.08 μm diameter on a silica substrate, and use the elastic constants (Ref. [29]) $E = 73$ GPa, $\nu = 0.17$, and work of adhesion (Ref. [22]) $w = 0.063\,\mathrm{J/m^2}$.

A. Rigid substrate

We plot numerical solutions of Eq. (9), to obtain the dispersion curves for the discrete model of interacting spheres on a rigid base, as shown in Fig. 3(a). In our description of a rigid substrate, we assume that no elastic waves propagate in the substrate, but allow local deformation at the points of contact for the purpose of the contact stiffness calculation; this preserves the same contact stiffnesses as in the elastic substrate analysis. We note that due to the periodicity of the system, all three branches have zero-group velocities at the edge of the first irreducible Brillouin zone [20] of the monolayer.

By substituting the solutions shown in Fig. 3(a) into the coefficient matrix of the corresponding algebraic system, we numerically determine the amplitudes of the sphere displacements, which we plot in Figs. 3(b)–3(d). By comparing the calculated displacements with the dispersion curves, we see that each branch takes on the character of its respective contact resonance in the limit $k \to 0$. One can see that each of the three modes generally involves both vertical and horizontal, as well as rotational motion (albeit the rotational component of mode II is quite small). The existence of the three modes with mixed displacements is a consequence of the inclusion of the rotational degree of freedom: without rotations, there would be two modes, one vertical and one horizontal.

We note that in the special case $K_S = 0$, the mode originating at ω_{HR} becomes purely horizontal and decouples from the other two modes. The remaining modes (characterized by vertical translation and rotation) are generally consistent with the results of Ref. [16], for the case of normal contact with a rigid surface and no bending rigidity. Since Ref. [16] considered hexagonal packing, the behavior is analogous at long wavelengths, but diverges at short wavelengths due to discrete lattice effects.

The dotted lines in Fig. 3(a) show dispersion curves calculated with the effective medium model as per Eq. (10).

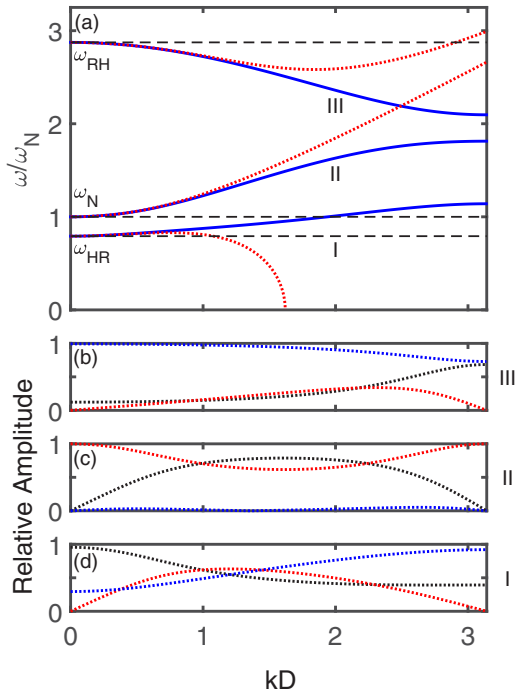

FIG. 3. (Color online) (a) Dispersion relation of a monolayer of microspheres adhered to a rigid base. Blue solid and red dotted lines denote, respectively, the discrete and effective medium monolayer descriptions. Black dashed lines denote the contact resonances. (b)–(d) relative amplitudes of the displacement variables Q (black dotted lines), Z (red dotted lines), and $R\theta$ (blue dotted lines), corresponding to the branches of the same numeral for the dispersion of the discrete monolayer adhered to the rigid base shown in (a). The amplitudes are normalized such that the sum of the squares is unity.

The effective medium approximation yields accurate results at long wavelengths but fails at shorter wavelengths with the unphysical behavior of the first mode, whose frequency goes to zero. At even shorter wavelengths, as shown in Fig. 4, the effective medium dispersion curves of modes II and III asymptotically approach straight lines with slopes given by

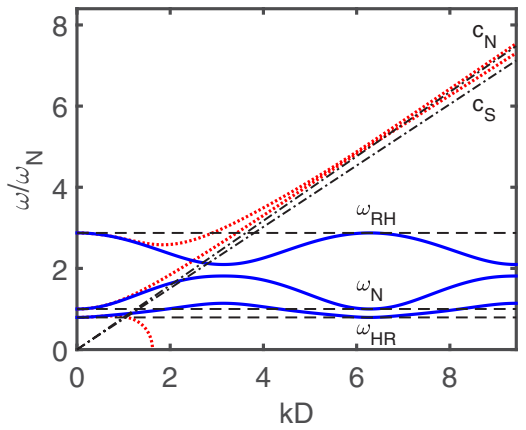

FIG. 4. (Color online) Dispersion relation of a monolayer of microspheres adhered to a rigid base, using an extended plotting range. Blue solid, red dotted, and black dashed lines are the same as in Fig. 3(a). Black dash-dotted lines denote the asymptotic slopes c_N and c_S.

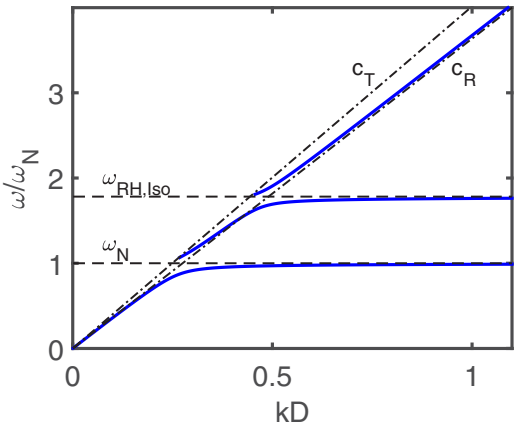

FIG. 5. (Color online) Dispersion relation of SAWs in an elastic half-space coupled to a monolayer of isolated microspheres, denoted by the blue solid lines. Black dashed lines denote the contact resonances, and black dash-dotted lines denote the transverse and Rayleigh waves speeds of the substrate.

c_N and c_S; such behavior has been described by Kosevich and Syrkin [15]. However, this asymptotic behavior is unphysical, because it arises as a short-wavelength asymptotic of a long-wavelength approximation. Indeed, as can be seen from the dispersion curves generated using the discrete model in Fig. 4, this asymptotic behavior does not occur in our system. Thus the inclusion of the first- and second-order spatial derivative terms of Eq. (7), while improving the accuracy of the effective medium model at long wavelengths, does not yield much additional understanding of the dynamics of the system.

B. Elastic substrate

1. *Isolated spheres*

We numerically solve Eq. (14) for the isolated spheres case using $G_S = 0$ and plot the resulting dispersion relation for the effective medium model, as shown in Fig. 5. This dispersion relation exhibits classic "avoided crossing" behavior [30] about the resonance frequencies ω_N and $\omega_{RH,Iso} = \sqrt{7/2}\,\omega_S$. In this model, surface acoustic waves (SAWs) in the substrate behave as classical Rayleigh waves at frequencies far from the contact resonances, and the dispersion curves follow the line corresponding to the substrate Rayleigh wave speed c_R [19]. Conversely, sphere motions dominate those of the substrate at frequencies close to the contact resonances. For phase velocities greater than c_T, which correspond to the region $\omega > c_T k$, the wave numbers that solve Eq. (13) are complex valued; these solutions are "leaky" modes for which energy leaves the surface of the substrate, and radiates into the bulk. This isolated spheres case is particularly applicable in systems where adhesion between particles is negligible, e.g., for macroscale particles without lateral compression where the dominant static compression is due to gravity and is between the particles and substrate; or for microscale particles, if the separation distance between particles is larger than the range of adhesion forces.

2. *Interacting spheres*

In Fig. 6(a), we plot numerical solutions of Eq. (14). The amplitudes of the sphere and substrate displacements are

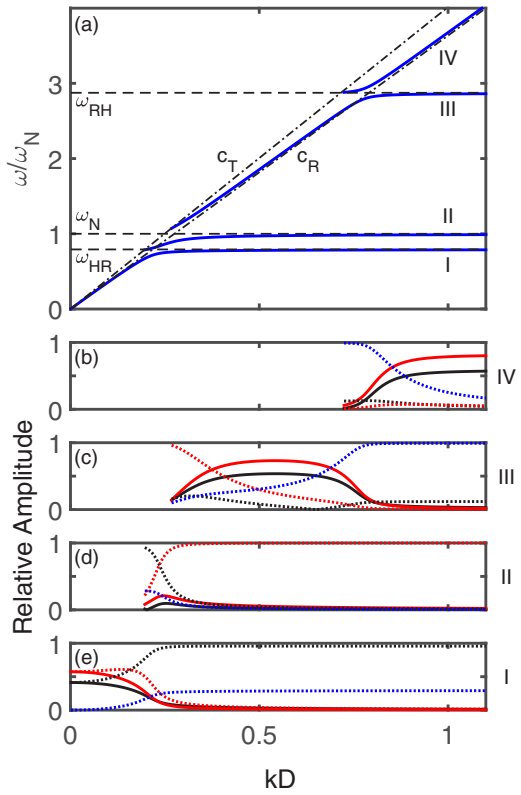

FIG. 6. (Color online) (a) Blue solid lines denote the dispersion relation of SAWs in an elastic halfspace coupled to a monolayer of interacting microspheres. Black dashed lines denote the contact resonances, and black dash-dotted lines denote wave speeds in the substrate. (b)–(e) relative amplitudes of the displacement variables u_0 (black solid lines), w_0 (red solid lines), Q (black dotted lines), Z (red dotted lines), and $R\theta$ (blue dotted lines), corresponding to the branch denoted by the same numeral in (a). The amplitudes are normalized such that the sum of the squares is unity.

calculated in the same manner as in Fig. 3, and are plotted in Figs. 6(b)–6(e). In Fig. 6(a), we observe features qualitatively similar to the dispersion relation for isolated spheres in Fig. 5, with the of a third avoided crossing at frequency ω_{HR}. The mode shapes reveal the ways in which each of the branches are influenced by the contact resonances, as well as long and short wavelength asymptotic behavior of our system. In the long-wavelength limit, the substrate motions closely resemble Rayleigh SAWs. Since the frequencies of waves in this regime are well below the contact resonances, the effect of the spheres is negligible, and the monolayer moves in phase with the substrate surface. At short wavelengths, it can be seen that the first, second, and third lowest branches exhibit motions dominated by the displacements Q, Z, and θ, respectively (each corresponding to a resonant mode of the monolayer), while the highest branch tends toward the Rayleigh SAW. The effects of proximity to the contact resonances are well illustrated, for example, by branch III of Fig. 6(a), which exhibits large vertical sphere motions at its starting point near ω_N, resembles the Rayleigh SAW as it approaches and crosses the c_R line, and transitions into large rotational sphere motions after the avoided crossing with ω_{RH}.

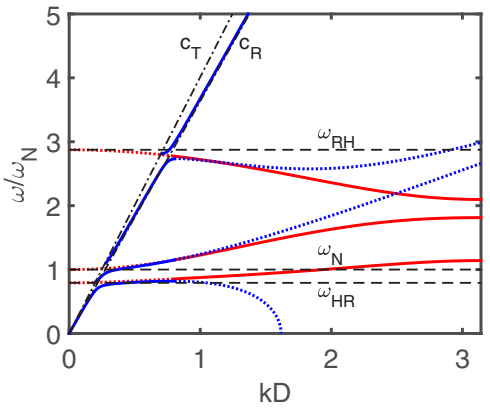

FIG. 7. (Color online) Blue lines denote the SAW dispersion relation with spatial derivative terms included and red lines denote the dispersion relation of a discrete monolayer adhered to a rigid base. Solid and dotted lines denote, respectively, valid and invalid ranges for the two models. Black dashed and dash-dotted lines are the same as in Fig. 3(a).

In order to examine the behavior of our system throughout the entire Brillouin zone, we superimpose the dispersion curves for the effective medium model of interacting spheres on an elastic base including higher order spatial derivative terms [the full Eq. (13)] with the dispersion curves for the discrete monolayer on a rigid substrate [Eq. (9)], as shown in Fig. 7. At long wavelengths, the discreteness of the monolayer is insignificant, and the dispersion is well described by the effective medium model. Furthermore, we note that at long wavelengths the dispersion curves calculated using the effective medium model including higher order terms shown in Fig. 7, only slightly deviate from the dispersion curves calculated using the effective medium model with the higher order terms neglected, which are shown in Fig. 6(a). The only noticeable effect is a downshift in frequency of the avoided crossing between the Rayleigh wave and the ω_{RH} resonance. Since the latter intersects at the highest wave vector of the three contact resonances, calculations with Eq. (14) are the least accurate. In Fig. 7, at short wavelengths (beyond the avoided crossings with the Rayleigh wave branch), the elasticity of the substrate has little effect on the dynamics, and the dispersion can be described using the discrete model for interacting spheres on a rigid substrate. We suggest that by "stitching together" the effective medium model for spheres on an elastic substrate with the discrete model for spheres on a rigid substrate, we can simultaneously capture the interaction of SAWs with the monolayer at long wavelengths and effects caused by the discreteness of the spheres at short wavelengths. Past the avoided crossings, the two sets of curves in Fig. 7 stitch together smoothly, resulting in a full picture of the monolayer dynamics on the elastic substrate.

V. EXPERIMENTAL IMPLICATIONS

We expect the presented results to be useful for predicting complex dynamic responses and extracting effective contact stiffnesses from measurements of acoustic dispersion in a manner similar to Boechler *et al.* [12]. The findings described

above invite questions, including whether our model of a square lattice is applicable to results on hexagonally packed monolayers, and why horizontal-rotational resonances were not observed in the experiment [12].

We believe that the assumption of the square lattice is not essential. For isolated spheres, Eqs. (7) and (8) with G_N and G_S set to zero can be obtained for any arrangement of the spheres, periodic or random, with the only parameter depending on the arrangement being the surface area per sphere A. For interacting spheres, the results generally do depend on the lattice structure and the propagation direction. However, the contact resonances given by Eq. (12) correspond to the $k = 0$ limit and, consequently, do not depend on the propagation direction. The relative positions of the three contact resonances may be different between a hexagonal and square packed lattice, but their presence should still be expected in both cases.

We suggest that the reasons why horizontal-rotational resonances were not observed in Ref. [12] may be the following. Since the measurements were not sensitive to horizontal motion, the ω_{RH} and ω_{HR} resonances could only be detected when they hybridized with SAWs near avoided crossings, and since the avoided crossings with ω_{RH} and ω_{HR} resonances are more narrow than the one with the ω_N resonance, they could have been missed. Furthermore, our model assumes that all spheres are either connected by identical springs or are isolated. If the contact stiffness between spheres were to vary widely (some neighboring spheres being in contact and others not, for example), then distinct resonances may be absent. In addition, the upper (ω_{RH}) resonance may have been outside the range of the measurements in Ref. [12]. Further experimental studies of monolayer dynamics in conjunction with exploration of ways to control sphere-to-sphere contacts should help resolve the discrepancy between the theory and experiment.

While the main focus of this work has been on microgranular monolayers, our theory is equally valid for nano- to macroscale systems. Contact resonances of isolated nanoparticles have been previously demonstrated for spheres as small as 120 nm in diameter, and their frequencies have been shown to scale in agreement with adhesive contact models based on Hertzian mechanics [31]. Conversely, at the macroscale, contact springs would be determined by gravity and, possibly, applied lateral static compression [9], rather than by adhesion forces. We note that several past experimental works on macroscale granular systems [9] have observed systematic upshifts in frequency relative to theoretical predictions, and have suggested uncertainties in material parameters and experimental setups, as well as deviations from Hertzian contact behavior as possible causes. The results from our model indicate that the presence of additional degrees of freedom and interactions between spheres and substrate may have also played a role. In the absence of the external lateral compression, highly nonlinear "sonic vacua" [3] should also be expected. Generally, as amplitudes are increased, interesting nonlinear dynamics are expected for granular monolayers due to nonlinearity of Hertzian contacts between the particles [3,6] and between the particles and the substrate [32].

VI. CONCLUSION

We have developed a model for wave propagation in granular systems composed of a monolayer of spheres on an elastic substrate. Our model expands on those used in previous works by including the elasticity of the substrate, horizontal and rotational sphere motions, shear coupling between the spheres and substrate, and interactions between adjacent spheres. We have shown that a monolayer of interacting spheres on a rigid substrate supports three modes involving vertical, horizontal, and rotational motion. In the long-wavelength limit, these modes yield three contact resonances, one purely vertical and two of mixed horizontal-rotational character. On an elastic substrate, these resonances hybridize with the Rayleigh surface wave yielding three avoided crossings. For isolated spheres, the frequency of the lower horizontal-rotational resonance, in the absence of bending rigidity, tends to zero and only two contact resonances with two respective avoided crossings remain.

By comparing the effective medium (valid for long wavelengths) to the discrete formulation of our model, we have demonstrated that for the presented microsphere monolayer example, the effective medium model can be used to describe the interaction of the contact resonances with the Rayleigh waves in the substrate, but loses accuracy at shorter wavelengths. In that case, the substrate can be considered rigid, and the discrete model is more appropriate. This model is scalable in that it can be adapted for use with nano- to macroscale systems, and provides a means to experimentally extract contact stiffnesses from dynamic measurements. Opportunities for future studies include exploration of analogous models for granular monolayers in the nonlinear regime, as well as analysis of the transverse modes of a granular monolayer or granular chain on a substrate. Further experiments on nano- to macroscale granular monolayers will help guide the modeling effort.

ACKNOWLEDGMENTS

The authors greatly appreciate discussions with Vitaly Gusev. S.P.W. and N.B. gratefully acknowledge support from the National Science Foundation (Grant No. CMMI-1333858) and the Army Research Office (Grant No. W911NF-15-1-0030). The contribution by A.A.M. was supported by the National Science Foundation Grant No. CHE-1111557.

[1] J. Duran, *Sand, Powders, and Grains: An Introduction to the Physics of Granular Materials* (Springer-Verlag, New York, 2000).

[2] H. Hinrichsen and D. E. Wolf, *The Physics of Granular Media* (WILEY-VCH Verlag GmbH & Co. KGaA, Weinheim, 2004).

[3] V. F. Nesterenko, *Dynamics of Heterogeneous Materials* (Springer-Verlag, New York, 2001).

[4] H. Hertz, J. Reine Angew. Math. **92**, 156 (1882).

[5] K. L. Johnson, *Contact Mechanics* (Cambridge University Press, Cambridge, 1985).

[6] G. Theocharis, N. Boechler, and C. Daraio, Nonlinear Periodic Phononic Structures and Granular Crystals, *Acoustic Metamaterials and Phononic Crystals* (Springer, Berlin, Heidelberg, 2013), pp. 217–251.

[7] L. Bonanomi, G. Theocharis, and C. Daraio, Phys. Rev. E **91**, 033208 (2015).

[8] A. N. Lazaridi and V. F. Nesterenko, Zh. Prikl. Mekh. Tekh. Fiz. **26**, 115 (1985); C. Coste, E. Falcon, and S. Fauve, Phys. Rev. E **56**, 6104 (1997); S. Job, F. Melo, A. Sokolow, and S. Sen, Phys. Rev. Lett. **94**, 178002 (2005); C. Daraio, V. F. Nesterenko, E. B. Herbold, and S. Jin, Phys. Rev. E **73**, 026610 (2006).

[9] N. Boechler and C. Daraio, in *Proceedings of the ASME 2009 Design Engineering Technical Conferences, San Diego, 2009* (ASME, New York, NY, 2009), pp. 271–276; N. Boechler, G. Theocharis, S. Job, P. G. Kevrekidis, M. A. Porter, and C. Daraio, Phys. Rev. Lett. **104**, 244302 (2010); N. Boechler, J. Yang, G. Theocharis, P. G. Kevrekidis, and C. Daraio, J. Appl. Phys. **109**, 074906 (2011).

[10] H. P. Rossmanith and A. Shukla, Acta Mech. **42**, 211 (1982); C. Daraio, D. Ngo, V. F. Nesterenko, and F. Fraternali, Phys. Rev. E **82**, 036603 (2010); J. Yang, S. Dunatunga, and C. Daraio, Acta Mech. **223**, 549 (2012).

[11] B. Gilles and C. Coste, Phys. Rev. Lett. **90**, 174302 (2003); A. Leonard, F. Fraternali, and C. Daraio, Exp. Mech. **53**, 327 (2011).

[12] N. Boechler, J. K. Eliason, A. Kumar, A. A. Maznev, K. A. Nelson, and N. Fang, Phys. Rev. Lett. **111**, 036103 (2013).

[13] A. R. Baghai-Wadji, V. P. Plessky, and A. V. Simonian, Sov. Phys. Acoust. **38**, 442 (1992).

[14] E. A. Garova, A. A. Maradudin, and A. P. Mayer, Phys. Rev. B **59**, 13291 (1999).

[15] Y. A. Kosevich and E. S. Syrkin, Phys. Lett. A **135**, 298 (1989).

[16] V. Tournat, I. Pèrez-Arjona, A. Merkel, V. Sanchez-Morchillo, and V. Gusev, New J. Phys. **13**, 073042 (2011).

[17] H. Pichard, A. Duclos, J-P. Groby, V. Tournat, and V. E. Gusev, Phys. Rev. B **86**, 134307 (2012).

[18] A. Merkel, V. Tournat, and V. Gusev, Phys. Rev. Lett. **107**, 225502 (2011).

[19] W. M. Ewing, W. S. Jardetzky, and F. Press, *Elastic Waves in Layered Media* (McGraw-Hill Book, New York, 1957).

[20] L. Brillouin, *Wave Propagation in Periodic Structures* (Dover, New York, 1953).

[21] V. M. Muller, B. V. Derjaguin, and Y. P. Toporov, Colloids Surf. **7**, 251 (1983); M. D. Pashley, *ibid.* **12**, 69 (1984).

[22] J. Israelachvili, *Intermolecular and Surface Forces* (Elsevier, Burlington, MA, 2011).

[23] R. D. Mindlin, J. Appl. Mech. **16**, 259 (1949).

[24] B. Bhushan, *Handbook of Micro/Nano Tribology* (CRC, Boca Raton, FL, 1999).

[25] R. Fuchs, T. Weinhart, J. Meyer, H. Zhuang, T. Staedler, X. Jiang, and S. Luding, Granular Matter **16**, 281 (2014).

[26] The quantity c_N is the long-wavelength longitudinal acoustic velocity in a suspended monolayer (or a 3D simple cubic lattice of spheres). The quantity c_S is the corresponding transverse velocity for the model case when rotations are disallowed. In a cubic crystal, in contrast to an isotropic solid, there are no restrictions on the ratio of transverse-to-longitudinal velocities in the [100] direction. While c_N and c_S can take any values if G_N and G_S are varied arbitrarily, within the Hertz-Mindlin theory c_S is just slightly below c_N.

[27] C. Dominik and A. G. G. M. Tielens, Philos. Mag. A **72**, 783 (1995).

[28] M. D. Murthy Peri and C. Cetinkaya, J. Colloid Interface Sci. **288**, 432 (2005).

[29] N. P. Bansat and R. H. Doremus, *Handbook of Glass Properties* (Academic Press, Orlando, FL, 1986).

[30] J. von Neumann and E. Wigner, Phys. Z. **30**, 467 (1929).

[31] Y. Guillet, B. Audoin, M. Ferrié, and S. Ravaine, Phys. Rev. B **86**, 035456 (2012).

[32] S. Wallen, C. Chong, P. G. Kevrekidis, and N. Boechler, in *Proceedings of the International Symposium on Optomechatronic Technologies, Seattle, 2014* (IEEE, New York, NY, 2014), pp. 15–17.